**Title**: Dysregulated alveolar epithelial maintenance in Hermansky-Pudlak syndrome pulmonary fibrosis

**Authors**: Joanna Y. Wang[1], Nigel S. Michki[2,3], Brandon J. Banaschewski[3], Ruby C. Pan[3], Jarod A. Zepp[3], David B. Frank[2,3], and Lisa R. Young[1,3]

**Author affiliations**: [1]Division of Pulmonary, Allergy, and Critical Care, Department of Medicine, Hospital of the University of Pennsylvania, Philadelphia, Pennsylvania, [2]Division of Cardiology, Department of Pediatrics, Children's Hospital of Philadelphia, Philadelphia, Pennsylvania, and [3]Division of Pulmonary and Sleep Medicine, Department of Pediatrics, Children's Hospital of Philadelphia, Philadelphia, Pennsylvania

**Corresponding author**: Lisa R. Young, M.D., Children's Hospital of Philadelphia, Leonard and Madlyn Abramson Pediatric Research Center, 3615 Civic Center Blvd, 4th Floor, Suite 416, Philadelphia, PA 19104. Phone: 215-590-3749, fax 215-590-3500, email: youngL5@chop.edu.

**Keywords**: epithelium, senescence, pulmonary fibrosis

**Grant Funding:** J.Y.W. receives support through an NIH Ruth L. Kirschstein National Research Service Award Institutional Research Training Grant (2-T32-HL-007586-36). J.A.Z. receives support through an NIH Pathway to Independence Award (R00-HL141684), an NIH Maximizing Investigators' Research Award (R35-GM146835), and an ATS/Hermansky-Pudlak Syndrome Network Research Grant. D.B.F receives support through an NIH Mentored Clinical Scientist Research Career Development Award (K08-HL140129). L.R.Y. receives support through an NIH Research Project Grant (R01-HL119503), an NIH Midcareer Investigator Award in Patient-Oriented Research (K24-HL143281), and the Rare Lung Diseases Frontier Program at the Children's Hospital of Philadelphia.

**Abstract**

Hermansky-Pudlak syndrome (HPS) is a genetic disorder of intracellular endosomal trafficking defects associated with pulmonary fibrosis. Double mutant HPS1/2 mice exhibit spontaneous fibrosis and single mutant HPS1 and HPS2 mice display increased fibrotic sensitivity. To identify mechanisms of AT2 cell dysfunction contributing to fibrosis in HPS, we examined lungs from aged HPS1/2 mice and observed regions of AT2 cell loss adjacent to areas of marked AT2 cell hyperplasia as compared to wild type (WT). Overall, there was accelerated loss of AT2 cells in HPS1/2, HPS1, and HPS2 mice with aging based on immunohistochemistry and lineage tracing studies. Lung organoids generated with HPS2 AT2 cells with WT fibroblasts were smaller in size and displayed significantly decreased colony forming efficiency compared to organoids with WT AT2 cells. Utilizing an H1N1 PR8 influenza model to examine AT2 cell regeneration after injury, there was a significant decrease in the percentage of proliferating AT2 cells in HPS1 and HPS2 mice compared to WT mice. RNA sequencing of AT2 cells isolated from unchallenged mice demonstrated upregulation of genes associated with proliferation and cellular senescence in HPS AT2 cells. Collectively, AT2 cells in HPS mice exhibit dysregulated proliferation with transcriptomic features suggesting subpopulations of senescent and hyperproliferative cells. Dysregulated maintenance of the alveolar epithelium with accelerated senescence and aberrant proliferation of AT2 cells appears to be a shared pathway underlying HPS and other sporadic and genetic forms of pulmonary fibrosis.

## Introduction

Pulmonary fibrosis, characterized by the replacement of lung tissue with scar and destruction of lung architecture, is the end stage manifestation of many lung diseases. Evidence points to dysfunctional alveolar epithelial type II (AT2) cells, which produce and store surfactant and act as stem cells in the alveolus, as a driver of fibrotic remodeling (1-3). Accelerated senescence of AT2 cells was first implicated in telomere-related diseases and increased endoplasmic reticulum (ER) stress identified in pulmonary fibrosis due to surfactant protein C gene mutations (4-6). Both of these mechanisms of cellular dysfunction, in addition to mitochondrial dysfunction and apoptosis, have subsequently been implicated in sporadic idiopathic pulmonary fibrosis (IPF) (4, 5, 7, 8). However, these pathways of cellular dysfunction are interconnected, and it remains unclear whether there are unifying mechanisms and final common pathways of AT2 cell dysfunction across different sporadic and genetic fibrotic lung diseases. Hermansky-Pudlak syndrome (HPS) is an autosomal recessive genetic disorder in which one of the primary manifestations is progressive pulmonary fibrosis, typically presenting in young adulthood in HPS1 and HPS4 and in childhood in HPS2 (9). Notably, pulmonary fibrosis has not been observed in the other subtypes of HPS, including HPS3. We originally demonstrated that HPS mutations in the alveolar epithelium underlie the fibrotic susceptibility, and studies from several groups have implicated apoptosis, impaired autophagy, and mitochondrial dysfunction in AT2 cells as potential contributing mechanisms (10-14).

In this study, we examined HPS AT2 cells with aging to elucidate mechanisms of AT2 cell dysfunction and their contribution to the fibrotic response. We utilized the double mutant HPS1/2 murine model, which exhibits spontaneous progressive fibrosis with aging, and compared the findings to those observed in the single mutant HPS1 and HPS2 models, which best reflect human disease genetics while exhibiting fibrotic sensitivity without spontaneous fibrosis (15, 16). Our studies demonstrate dysregulated maintenance of the alveolar epithelium in HPS, with heterogenous regions of AT2 cell loss and hyperplasia and overall accelerated loss of AT2 cells with aging in HPS1, HPS2, and HPS1/2 mice. Further, transcriptomic signatures suggest emergence of subpopulations of hyperproliferative and

senescent HPS AT2 cells. Lastly, we provide evidence of impaired proliferation of HPS1 and HPS2 AT2 cells in an *in vivo* influenza lung injury model, with abnormalities also in HPS2 AT2 cells in an *ex vivo* lung organoid model. Taken together, these data reveal that dysregulated maintenance of the alveolar epithelium with accelerated senescence and aberrant proliferation of AT2 cells contributes to pulmonary fibrosis in HPS, suggesting shared mechanisms of disease across sporadic and genetic fibrotic lung diseases.

## Materials and Methods

*Animal studies and treatment*

Naturally occurring HPS1, HPS2, and HPS3 mice, which harbor mutations in the mouse homologues of the *HPS1*, *AP3B1*, and *HPS3* genes, respectively, were maintained on the C57BL6/J background (17). Transgenic HPS2 mice, with partial correction of AP3b1 in the lung epithelium, were described previously (10). Double mutant HPS1/2 mice were generated by mating homozygous HPS1 and homozygous HPS2 mice (16, 18, 19). WT Sftpc$^{CreERT2/+}$;R26R$^{EYFP/+}$ (Jackson Laboratory, strain # 006148) mice were provided by Dr. Jarod Zepp and generated by Dr. Howard Chapman (University of California, San Francisco) as described previously, and bred with HPS1 and HPS2 mice to generate HPS1 Sftpc$^{CreERT2/+}$;R26R$^{EYFP/+}$ and HPS2 Sftpc$^{CreERT2/+}$;R26R$^{EYFP/+}$ mice, respectively (20). All procedures for animal experiments were performed under the guidance of and in compliance with all ethical regulations of the Children's Hospital of Philadelphia Institutional Animal Care and Use Committee (IACUC). Four- to 48-week-old animals of both sexes were used for experiments, as specified. For lineage trace experiments, four-week-old Sftpc$^{CreERT2/+}$;R26R$^{EYFP/+}$ mice were administered tamoxifen (200 mg/kg body weight) in corn oil via oral gavage for three consecutive days. For cell proliferation experiments, 5-ethynyl-2'-deoxyuridine (EdU) was dissolved in filtered PBS and administered via intraperitoneal injection at a dose of 50 mg/kg four hours prior to euthanasia and isolation of lungs.

*Histology and immunohistochemistry*

Lungs were harvested at a constant pressure of 30 cm $H_2O$ and were fixed overnight at 4°C in 4% paraformaldehyde. For whole-mount imaging, lung tissue was washed in PBS, embedded in 4% low-melting agarose, and sectioned at 150 µm thickness. For paraffin embedding, lung tissue was washed in PBS, dehydrated in a graded series of ethanol washes, embedded in paraffin wax, and sectioned at 7 µm thickness. Hematoxylin and eosin (H&E) and Masson's trichrome staining were performed according to standard procedures. Immunohistochemistry (IHC) was performed with antibodies for prosurfactant protein-C (proSP-C) (Invitrogen, PA5-71680), Nkx2.1 (Invitrogen, MA5-13961), and GFP (Aves Labs, GFP-1020). EdU staining was performed with the Click-iT EdU cell proliferation kit according to the manufacturer's instructions (Invitrogen). Slides were mounted in Vectashield Antifade Mounting Medium (Vector Labs). Images were captured using a Leica confocal microscope. All image quantification was performed on serial confocal images from z-stack max intensity composites. For paraffin-embedded sections, 10 images per slide were randomly selected via the 405 nm (DAPI) channel and captured for quantification. Manual counting of DAPI nuclei, proSP-C positive cells, Nkx2.1 positive cells, and GFP positive cells was performed in a blinded fashion.

*Alveolar epithelial type II cell isolation*

Murine lung single cell suspensions were prepared by intratracheal infusion of dispase and agarose, dispase digestion, and serial filtration through 70-µm and 40-µm cell strainers as described previously (21). AT2 cells were subsequently isolated by fluorescence activated cell sorting (FACS) using antibodies for cell surface markers via negative selection for CD45, positive selection for EpCAM, and negative selection for β4 integrin (CD104) (Biolegend) (20, 22). Samples of the AT2 cell suspensions were fixed and stained for proSP-C, with confirmation of purity > 95%.

*Lung organoid assays*

AT2 cells were isolated as described above. Live cell numbers were verified using a hemocytometer and Trypan Blue Solution. In each technical replicate, 5,000 AT2 cells were combined with 50,000 primary

outgrowth wild type (WT) murine lung fibroblasts in 50% Matrigel (growth factor reduced, phenol-red free) (Corning) and in small airway growth media (Lonza) with the following additives: insulin, transferrin, bovine pituitary extract, retinoic acid, and gentamicin (all from Lonza), with cholera toxin (Sigma) and FBS (Corning). The ROCK inhibitor thiazovivin (Stem Cell) was included in the media for the first two days and fresh media was added every two days. Images were captured over the course of culture using a Leica Thunder microscope. Images were processed in ImageJ with thresholding and then binarized. All organoids within a well were used for quantification. Organoid number and size were quantified using the analyze particles function in ImageJ with a cutoff of 1500 $\mu m^2$. Colony forming efficiency was calculated by dividing the organoid number by the number of input AT2 cells (5,000). Organoids were fixed at the time points specified and stained with antibodies for proSP-C (Invitrogen, PA5-71680) and Ager (Rage) (R&D Systems, MAB1179).

*Influenza infection*

H1N1 PR8 influenza virus was generously provided by Dr. Andrew Vaughan (University of Pennsylvania) and titration by $TCID_{50}$ for infectivity was performed in MDCK cells (23). HPS2 and WT mice, aged 8 to 12-weeks old, were anesthetized with 4% isoflurane in 100% $O_2$ via an anesthesia vaporizer system, and H1N1 PR8 influenza was delivered intratracheally at a dose of 100 U diluted in 50 µl PBS. In a subsequent experiment, HPS1 and WT mice, aged 8-12 weeks old, were anesthetized with xylazine and ketamine via intraperitoneal injection, H1N1 PR8 influenza was delivered intranasally at a dose of 100 U diluted in 50 µl PBS. Mouse weights were tracked daily starting from the day of infection. Mice were shaved and pulse oximetry measurements were obtained using MouseOx Plus (Starr Life Sciences) every second or third day starting from the day of infection for the time points noted.

*Lung injury assessment*

To define regions of lung injury after influenza infection, an unbiased image classification machine learning model was used on H&E-stained sections to cluster image pixels by staining intensity, similar to

previously described methodology (24, 25). Three regions of injury were defined: severely injured, mildly injured, and uninjured.

*Picrosirius red staining*

Staining for collagen was performed using picrosirius red staining kit per the manufacturer's instructions (Polysciences Inc.). Digital morphometric measurements and collagen quantitation were performed as previously described (26). Naïve WT lung tissue was normalized to a collagen area of 3.0%.

*Bulk RNA sequencing*

Total RNA was extracted from freshly sorted AT2 cells using the RNeasy Micro Kit (Qiagen) and stored at -80°C. Frozen total RNA was sent to Genewiz/Azenta Life Sciences (NJ, USA) for bulk mRNA-sequencing, using their standard RNA-seq service. Reads in FASTQ format were aligned to the NCBI mouse genome (mm10/GRCm38) and quantified at the gene level using the nf-core/rnaseq v3.8.1 Nextflow pipeline (27, 28). Differential gene expression analysis was performed using DESeq2 and scanpy (29, 30). Aggregate gene set scores were calculated using the JASMINE scoring metric (31).

*β-galactosidase staining*

AT2 cells were deposited on glass slides by cytospin centrifugation at 500 rpm for 5 minutes. Fixation and staining were performed using a β-galactosidase staining kit per the manufacturer's instructions at pH 6.0 (Cell Signaling).

*Statistics*

Statistical analyses were performed with GraphPad Prism. Student's t-test were used for comparison between groups for parametric data and Mann-Whitney U-test for non-parametric data. Results are presented as mean ± SEM. $p$ values < .05 were considered significant. For multiple comparisons, the

Benjamini-Hochberg procedure was utilized with a false discovery rate of 0.05. Adjusted $p$ values < .05 were considered significant.

## Results

*Loss of AT2 cells with aging in HPS mice*

We first confirmed that double mutant HPS1/2 mice generated in our colony developed spontaneous, progressive fibrosis with aging as previously described (**Supplemental Figure 1A-D**) (16). We then utilized IHC for the AT2 cell marker, proSP-C, to examine the alveolar epithelium in aged HPS1/2 mice compared to WT. In addition to regions of marked AT2 cell hyperplasia as previously described, we also observed regions of near total proSP-C$^+$ AT2 cell loss (**Figure 1A**). To measure AT2 cell dynamics with aging *in situ*, AT2 cells in WT and HPS1/2 mice at 4, 8, 24, and 48 weeks of age were quantified via IHC for proSP-C. Starting at 8 weeks of age, we found a significant decrease in the percentage of proSP-C$^+$ AT2 cells per total DAPI positive cells in HPS1/2 mice, with 10.3 ± 0.4% in HPS1/2 mice compared to 13.9 ± 0.3% in WT (adjusted $p$ = .02). These percentages corresponded to a mean of 56.8 ± 10.4 AT2 cells per high powered field (hpf) in WT mice and 31.0 ± 10.2 cells per hpf in HPS1/2 mice ($p$ < .0001). There was progressive loss of AT2 cells with aging in HPS1/2 mice, which exhibited 8.1 ± 0.5% proSP-C$^+$ cells at 48 weeks of age. Of note, there was also a decrease in AT2 cells in WT mice with aging, with 11.5 ± 0.2% at 48 weeks of age ($p$ = .002).

Significant AT2 cell loss with aging was also seen in single mutant HPS1 and HPS2 mice, by 8 weeks and 24 weeks of age, respectively (**Figure 1B, 1D-E**). At 8 weeks of age, HPS1 mice exhibited 12.1 ± 0.3% proSP-C$^+$ cells compared to 13.9 ± 0.3% in WT (adjusted $p$ = .029); by 24 weeks of age, HPS2 mice displayed 9.3 ± 0.4% compared to 13.3 ± 0.3% in WT (adjusted $p$ = .016). To account for the possibility of immune cells and other cell types present in HPS mice that could alter the total cell count and contribute to lower percentages of proSP-C$^+$ cells, we also quantified the percentage of proSP-C$^+$ cells per total epithelial cells as denoted by Nkx2.1$^+$ staining. There was a significant decrease in the percentage of

proSP-C$^+$, Nkx2.1$^+$ cells in HPS1 vs. WT mice at 8 weeks of age (72.2 ± 3.2% vs. 78.2 ± 3.5, $p$ = .046) and in HPS2 vs. WT mice at 24 weeks of age (65.0 ± 2.4% vs. 76.1 ± 3.9%, $p$ = .0029) (**Supplemental Figure 2A-D**). In contrast, in HPS3 mice, significant loss of AT2 cells was not observed by 24 weeks of age compared to WT (**Supplemental Figure 3A-B**). Furthermore, in transgenic epithelial-corrected HPS2 mice, AT2 cell numbers were significantly greater compared to HPS2 mice at 24 weeks of age (**Supplemental Figure 3A, 3C**). No TUNEL-positive apoptotic AT2 cells were detected in WT or HPS mice across the same timepoints (data not shown).

To confirm these findings based on proSP-C expression and further investigate the etiology of AT2 cell loss, we generated WT, HPS1, and HPS2 Sftpc$^{CreERT2/+}$;R26R$^{EYFP/+}$ mice and performed lineage tracing of AT2 cells. Recombination with tamoxifen was induced at four weeks of age, prior to the timepoint where we observed onset of significant AT2 cell loss based on proSP-C immunostaining (**Figure 1B-E**). Quantification of the number of lineage-labeled AT2 cells (GFP$^+$, proSP-C$^+$) again demonstrated significant loss of AT2 cells with aging, similar to that observed in WT, HPS1, and HPS2 mice (**Figure 1D-E**). HPS1 Sftpc$^{CreERT2/+}$;R26R$^{EYFP/+}$ mice exhibited 11.8 ± 0.2% GFP$^+$, proSP-C$^+$ cells compared to 14.4 ± 0.8% in WT Sftpc$^{CreERT2/+}$;R26R$^{EYFP/+}$ at 8 weeks of age (adjusted $p$ = .003) (**Figure 2B**). HPS2 Sftpc$^{CreERT2/+}$;R26R$^{EYFP/+}$ mice exhibited 12.9 ± 1.1% GFP$^+$, proSP-C$^+$ cells compared to 14.4 ± 0.8% in WT Sftpc$^{CreERT2/+}$;R26R$^{EYFP/+}$ at 8 weeks of age ($p$ = .034) (**Figure 2C**). Notably, all proSP-C$^+$ cells expressed GFP, and lineage-labeled GFP$^+$ cells that did not express proSP-C were not detected at any age (**Figure 2A**).

*Lung organoids generated from AT2 cells from HPS2 mice demonstrate attenuated size and growth.*
As we observed regions of AT2 cell hyperplasia with overall AT2 cell loss, we employed an *ex vivo* organoid model to evaluate AT2 cell proliferation in HPS mice (24). As the phenotype of AT2 cell loss was seen in single mutant HPS1 and HPS2 mice, as well as the double mutant HPS1/2 mice, we utilized AT2 cells from single mutant HPS1 and HPS2 mice at 8 weeks of age for organoid assays. We generated

lung organoids from WT AT2 cells with WT lung fibroblasts and organoids from HPS1 and HPS2 AT2 cells with WT fibroblasts. Compared to lung organoids generated with WT AT2 cells, those with HPS2 AT2 cells were smaller in size and displayed significantly decreased colony forming efficiency (CFE) over 21 days of culture at 2.5 ± 0.4% compared to 4.2 ± 0.4% in WT organoids ($p$ = .043) (**Figure 3A-D**). In contrast, organoids generated from HPS1 AT2 cells demonstrated comparable size and growth compared to those generated with WT AT2 cells (**Figure 3A-D**).

*HPS1 and HPS2 mice display impaired AT2 cell proliferation after influenza infection*

To further evaluate whether proliferation is impaired in HPS AT2 cells *in vivo*, we employed an influenza model to examine AT2 cell regeneration after acute injury (22, 24). We performed an initial set of experiments with WT and HPS2 mice, then modified the method of anesthesia and influenza delivery to optimize dosing consistency for a subsequent set of experiments with WT and HPS1 mice. Weight change and oxygen saturation were comparable in WT and HPS1 mice during the first 10 days post-infection (dpi); subsequently, oxygen saturations trended lower in HPS1 and HPS2 mice though no mortality difference was observed (**Figure 4A-B, 5A-B**). Given the heterogeneous nature of influenza-induced lung injury and to ensure appropriate quantification and comparison, a computational image analysis approach was used to cluster image pixels based on the intensity of H&E staining to define three regions: severely injured, mildly injured, and uninjured (**Figure 4C, 5C**). To examine epithelial regeneration after acute influenza infection, we quantified the percentage of $EdU^+$, proSP-$C^+$ cells in WT vs. HPS1 and WT vs. HPS2 mice in severely injured and mildly injured regions at 14 dpi. There was a significant decrease in the percentage of proliferating AT2 cells in HPS1 mice compared to WT in severely injured regions, with 16.4 ± 4.5% $EdU^+$, proSP-$C^+$ in severely injured regions in HPS1 mice compared to 22.8 ± 3.2% in WT ($p$ = .015), and mildly injured regions, with 16.8 ± 3.0% in HPS1 mice compared to 25.1 ± 7.3% in WT ($p$ .020) (**Figure 4D-E**). There was also a significant decrease in the percentage of proliferating AT2 cells in HPS2 mice compared to WT in severely injured, but not mildly injured regions, with 24.8 ± 2.0% $EdU^+$, proSP-$C^+$ in severely injured regions in HPS2 mice compared to 33.5 ± 4.2% WT ($p$ = .014) (**Figure 5D-**

**E**). No difference in the area formed by keratin 5 (Krt5)-expressing cells in WT vs. HPS2 mice and WT vs. HPS1 mice was detected at 14 dpi (**Supplemental Figure 4A-C**).

*Transcriptomic analysis suggests emergence of subpopulations of senescent and hyperproliferative AT2 cells*

To identify mechanisms contributing to aberrant AT2 cell proliferation and pulmonary fibrosis, we examined the transcriptome of AT2 cells isolated from WT and HPS1/2 mice at 8 and 48 weeks of age as well as HPS1 and HPS2 mice at 8 weeks of age by bulk RNA sequencing. By FACS, there was a significant decrease in the percentage of AT2 cells captured from HPS mice compared to WT (**Supplemental Figure 5A-D**). Differential gene expression analysis and over-representation analysis (ORA) demonstrated upregulation of genes associated with immune cell activation and cell cycle regulation in HPS AT2 cells (**Supplemental Figure 6A-I**). Notably, markers of both cellular senescence and cell proliferation were upregulated in HPS1, HPS2, and HPS1/2 AT2 cells (**Figure 6A-C**). As cells are unlikely to simultaneously expression senescence markers and the proliferation marker Mki67, this suggests the emergence of distinct subpopulations of senescent and hyperproliferative AT2 cells in HPS mice (32). In addition, a subset of AT2 cells isolated from HPS1/2 mice at 8 and 48 weeks of age stained positive for β-galactosidase, a marker for senescent cells, whereas no β-galactosidase activity was detected in AT2 cells from WT mice at any age (**Figure 6D**).

## Discussion

Across sporadic and genetic forms of pulmonary fibrosis, AT2 cell dysfunction appears to play a central role in disease pathogenesis. However, the exact mechanisms by which AT2 dysfunction drives the fibrotic response in HPS-PF are incompletely understood, and there has been debate about whether mechanisms in HPS are distinct from IPF and other heritable forms of pulmonary fibrosis (1, 2). In this study, we demonstrate that maintenance of the alveolar epithelium is dysregulated in HPS both with aging and lung injury. Through immunostaining and lineage tracing, we confirmed overall loss of AT2 cells

with aging in HPS models associated with fibrosis. In contrast, HPS3 mice, a model for a subtype of HPS not associated with pulmonary fibrosis, did not exhibit AT2 cell loss. Finally, we found transcriptomic signatures of subpopulations of senescent and hyperproliferative HPS AT2 cells, consistent with the histologic findings of regions of AT2 cell loss and hyperplasia and the alterations in HPS AT2 cell proliferative capacity observed in the organoid and influenza models. These findings provide insight into the mechanisms by which HPS AT2 cells may contribute to fibrotic remodeling and highlight shared common pathways of alveolar epithelial dysfunction between HPS-PF and other forms of pulmonary fibrosis.

Under homeostatic conditions, AT2 cells are largely quiescent yet some degree of proliferation is required to maintain the alveolar epithelium (33). In IPF, disruption of the alveolar epithelium is a key feature, with both increased AT2 cell apoptosis and AT2 cell hyperplasia (2, 7, 34, 35). Both rare and common variants in *KIF15*, a kinesin involved in regulation of mitosis, increase risk for IPF, and *KIF15* expression is decreased in replicating lung epithelial cells in patients with IPF (36). AT2 cell proliferation is also dysregulated in HPS, which may result in failure to maintain the alveolar epithelium. We observed decreased rates of proliferation in HPS2 AT2 cells in both an organoid model and an influenza injury model; however, HPS1 AT2 cells appeared to perform comparably to WT AT2 cells in an organoid model but exhibited impaired proliferation after injury in an influenza model. This may reflect differences in the consequences of the HPS1 and HPS2 mutations on AT2 cell function as well as the models utilized to study cell proliferation and regeneration. The differences in AT2 cell proliferation in injury zones suggests that the HPS mutations have divergent effects on AT2 cell subpopulations, particularly those that function as alveolar epithelial progenitor cells after severe vs. more mild forms of lung injury (24, 25). Notably, while there was overall loss of AT2 cells with aging in all the HPS murine models, we did not observe AT2 cell apoptosis in any of the HPS models up to 48 weeks of age. Previous studies have described increased AT2 cell apoptosis in bleomycin-challenged but not naïve HPS1 and HPS2 mice (13, 15). Taken together, these data suggest that loss of AT2 cells may be a consequence of defects in

proliferation and support the theory that AT2 cell apoptosis is neither necessary nor sufficient to induce fibrosis (35).

Aberrant AT2 cell proliferation may result in part from accelerated senescence, which has been shown to drive the fibrotic response in telomere disorders (37, 38). In an experimental murine model, loss of function of SIN3 transcription regulator homolog A (Sin3a), a regulator of Trp53 acetylation, in AT2 cells was sufficient to induce AT2 cell senescence and spontaneous, progressive fibrosis (39). Furthermore, induction of AT2 cell senescence via loss of Sin3a resulted in impaired proliferation and progressive loss of AT2 cells. Senescent cells are thought to promote fibrosis through adoption of the senescence-associated secretory phenotype (SASP), producing cytokines, chemokines, and growth factors, which activate immune cells and fibroblasts (40). Both epithelial cells and fibroblasts in lung tissue from patients with IPF and bleomycin-challenged mice exhibit increased expression of SASP markers (40). Our findings in HPS mice with features of AT2 cell senescence, impaired proliferative response, and ultimately AT2 cell loss with aging are consistent with these models. Prior studies demonstrated that HPS AT2 cells have excess production of monocyte chemoattractant protein-1 (MCP-1), a SASP factor, and epithelial-specific deletion of MCP-1 reduced fibrotic susceptibility in HPS mice (41, 42). HPS1 patients have also been shown to have elevated levels of MCP-1 in bronchoalveolar lavage (BAL) fluid that correlate with lung disease severity (43).

The mechanisms by which the HPS endosomal trafficking mutations result in senescence in a subset of AT2 cells are unknown. Unlike findings in telomere disorders and familial IPF, telomere shortening has not been observed in peripheral blood mononuclear cells of individuals with HPS-PF (44). While the HPS mutations could produce cell cycle defects that directly result in cell cycle arrest, it is also possible that the mutations contribute to other forms of cellular dysfunction, including mitochondrial dysfunction and aberrant autophagy, which can induce cellular senescence (11, 14). These pathways have been implicated in other fibrotic lung diseases and may be part of the interconnecting pathways contributing to AT2 cell senescence in HPS. Regardless, there may be an additive effect of the HPS1 and HPS2 mutations that results in markedly accelerated senescence in double mutant HPS1/2 AT2 cells that

could underlie divergent phenotypes observed, with fibrotic sensitivity in HPS1 and HPS2 mice and spontaneous fibrosis in HPS1/2 mice.

In addition to subpopulations of senescent AT2 cells, fibrotic remodeling in the lungs appears to be characterized by a subset of hyperproliferative AT2 cells (2). AT2 cell hyperplasia is a classic histopathologic feature of IPF, which has also been previously observed in HPS (18, 34, 45, 46). In IPF, hyperproliferative AT2 cells are thought to compensate for ongoing epithelial cell dysfunction and appear to contribute to fibrotic remodeling through release of mediators, including matrix metalloproteinases and cytokines, and recruitment of fibroblasts (2, 3). In mice challenged with bleomycin, treatment with an inhibitor of deoxycytidine kinase (DCK), an enzyme important for DNA replication, resulted in decreased epithelial cell proliferation and an attenuated fibrotic response. Furthermore, whole lung transcript levels of MCP-1, CCR2, and MMP13 were significantly decreased in bleomycin-challenged mice after DCK inhibition (47). In HPS, in addition to the pathogenic role of MCP-1, expression of MMPs have also been found to be elevated in the alveolar epithelium (48). However, the contribution of hyperplastic AT2 cells to the fibrotic response in HPS remains unclear.

Given the role of AT2 cells as progenitor cells within the alveolus, another important consequence of AT2 cell dysfunction is impaired transdifferentiation. Several single-cell RNA sequencing studies of lung tissue from bleomycin-challenged mice and patients with IPF lung tissue have identified epithelial cell subpopulations with unique transcriptional signatures, lacking canonical marker genes for AT2 or AT1 cells (49, 50). Trajectory inference analysis and lineage tracing studies suggested that these intermediate or transitional cells result from impaired transdifferentiation of AT2 cells into AT1 cells. These cells also demonstrated enrichment in p53, DNA damage, and cellular senescence pathways (49, 50). Lineage tracing of AT2 cells in HPS1 and HPS2 mice, the models which best represent of HPS human disease genetics, did not reveal transitional cell populations that would presumably express the lineage marker EYFP without expression of proSP-C. However, given the challenges in detecting GFP expression in AT1 cells of irregular morphology, it remains possible that technical issues impacted

identification of rare transitional cells (20). Furthermore, as lineage tracing was performed in single mutant models without injury challenges, a role for transitional cells in HPS-PF cannot be fully excluded.

As a monogenic disorder with several murine models that recapitulate key features of the disease, HPS presents a unique opportunity for the study of progressive pulmonary fibrosis. Our findings provide insight into the role of AT2 cells in the pathogenesis of HPS-PF and suggest that there are common mechanisms, including accelerated senescence of AT2 cells, driving the fibrotic response in sporadic and genetic forms of pulmonary fibrosis. The relative contributions of rare and common genetic risk variants, in conjunction with environmental exposures, may vary across different forms of pulmonary fibrosis, but it is likely that these pathways converge, resulting in failure to maintain alveolar epithelial integrity. While we observed aberrant HPS AT2 cell proliferation and transcriptomic features suggesting subpopulations of senescent and hyperproliferative AT2 cells, additional studies at a single-cell resolution may further define and characterize the subpopulations of epithelial cells in HPS. We also found features of transcriptomic and functional divergence between HPS1 and HPS2 AT2 cells, highlighting that the differences exist between HPS subtypes which may help illuminate key aspects of HPS biology. Finally, it remains unclear if accelerated senescence or aberrant proliferation of AT2 cells is sufficient to drive the fibrotic response in HPS-PF. Given the shared pathways that have been identified, further study of the role of alveolar epithelial dysfunction in HPS-PF should have broad applicability across fibrotic lung diseases.

**Acknowledgements**: We thank Mary Kate Goldy and Heather Kelley for technical assistance. The authors also thank Dr. Andrew Vaughan, Dr. Jeremy Katzen, Dr. Luis Rodriguez, and Dr. Michael Beers for experimental guidance.

**References**

1. Parimon T, Yao C, Stripp BR, Noble PW, Chen P. Alveolar epithelial type II cells as drivers of lung fibrosis in idiopathic pulmonary fibrosis. International journal of molecular sciences. 2020;21(7):2269.

2. Katzen J, Beers MF. Contributions of alveolar epithelial cell quality control to pulmonary fibrosis. J Clin Invest. 2020;130(10):5088-99.

3. Selman M, Pardo A. The leading role of epithelial cells in the pathogenesis of idiopathic pulmonary fibrosis. Cell Signal. 2020;66:109482.

4. Lawson WE, Crossno PF, Polosukhin VV, Roldan J, Cheng D, Lane KB, Blackwell TR, Xu C, Markin C, Ware LB. Endoplasmic reticulum stress in alveolar epithelial cells is prominent in IPF: Association with altered surfactant protein processing and herpesvirus infection. American Journal of Physiology-Lung Cellular and Molecular Physiology. 2008;294(6):L1119-26.

5. Armanios MY, Chen JJ, Cogan JD, Alder JK, Ingersoll RG, Markin C, Lawson WE, Xie M, Vulto I, Phillips III JA. Telomerase mutations in families with idiopathic pulmonary fibrosis. N Engl J Med. 2007;356(13):1317-26.

6. Katzen J, Wagner BD, Venosa A, Kopp M, Tomer Y, Russo SJ, Headen AC, Basil MC, Stark JM, Mulugeta S. An SFTPC BRICHOS mutant links epithelial ER stress and spontaneous lung fibrosis. JCI insight. 2019;4(6)

7. Korfei M, Ruppert C, Mahavadi P, Henneke I, Markart P, Koch M, Lang G, Fink L, Bohle R, Seeger W. Epithelial endoplasmic reticulum stress and apoptosis in sporadic idiopathic pulmonary fibrosis. American journal of respiratory and critical care medicine. 2008;178(8):838-46.

8. Bueno M, Lai Y, Romero Y, Brands J, Croix CMS, Kamga C, Corey C, Herazo-Maya JD, Sembrat J, Lee JS. PINK1 deficiency impairs mitochondrial homeostasis and promotes lung fibrosis. J Clin Invest. 2015;125(2):521-38.

9. Hengst M, Naehrlich L, Mahavadi P, Grosse-Onnebrink J, Terheggen-Lagro S, Skanke LH, Schuch LA, Brasch F, Guenther A, Reu S. Hermansky-Pudlak syndrome type 2 manifests with fibrosing lung disease early in childhood. Orphanet journal of rare diseases. 2018;13(1):1-11.

10. Young LR, Gulleman PM, Bridges JP, Weaver TE, Deutsch GH, Blackwell TS, McCormack FX. The alveolar epithelium determines susceptibility to lung fibrosis in Hermansky-Pudlak syndrome. American journal of respiratory and critical care medicine. 2012;186(10):1014-24.

11. Ahuja S, Knudsen L, Chillappagari S, Henneke I, Ruppert C, Korfei M, Gochuico BR, Bellusci S, Seeger W, Ochs M. MAP1LC3B overexpression protects against Hermansky-Pudlak syndrome type-1-induced defective autophagy in vitro. American Journal of Physiology-Lung Cellular and Molecular Physiology. 2016;310(6):L519-31.

12. Cuevas-Mora K, Roque W, Shaghaghi H, Gochuico BR, Rosas IO, Summer R, Romero F. Hermansky-Pudlak syndrome-2 alters mitochondrial homeostasis in the alveolar epithelium of the lung. Respiratory research. 2021;22(1):1-11.

13. Zhou Y, He CH, Herzog EL, Peng X, Lee C, Nguyen TH, Gulati M, Gochuico BR, Gahl WA, Slade ML. Chitinase 3–like–1 and its receptors in Hermansky-Pudlak syndrome–associated lung disease. J Clin Invest. 2015;125(8):3178-92.

14. Cinar R, Park JK, Zawatsky CN, Coffey NJ, Bodine SP, Abdalla J, Yokoyama T, Jourdan T, Jay L, Zuo MXG. CB1R and iNOS are distinct players promoting pulmonary fibrosis in Hermansky-Pudlak syndrome. Clinical and Translational Medicine. 2021;11(7):e471.

15. Young LR, Pasula R, Gulleman PM, Deutsch GH, McCormack FX. Susceptibility of Hermansky-Pudlak mice to bleomycin-induced type II cell apoptosis and fibrosis. American journal of respiratory cell and molecular biology. 2007;37(1):67-74.

16. Mahavadi P, Korfei M, Henneke I, Liebisch G, Schmitz G, Gochuico BR, Markart P, Bellusci S, Seeger W, Ruppert C. Epithelial stress and apoptosis underlie Hermansky-Pudlak syndrome–associated interstitial pneumonia. American journal of respiratory and critical care medicine. 2010;182(2):207-19.

17. Li W, Rusiniak ME, Chintala S, Gautam R, Novak EK, Swank RT. Murine Hermansky–Pudlak syndrome genes: Regulators of lysosome-related organelles. Bioessays. 2004;26(6):616-28.

18. Lyerla TA, Rusiniak ME, Borchers M, Jahreis G, Tan J, Ohtake P, Novak EK, Swank RT. Aberrant lung structure, composition, and function in a murine model of Hermansky-Pudlak syndrome. American Journal of Physiology-Lung Cellular and Molecular Physiology. 2003;285(3):L643-53.

19. Guttentag SH, Akhtar A, Tao J, Atochina E, Rusiniak ME, Swank RT, Bates SR. Defective surfactant secretion in a mouse model of Hermansky-Pudlak syndrome. American journal of respiratory cell and molecular biology. 2005;33(1):14-21.

20. Chapman HA, Li X, Alexander JP, Brumwell A, Lorizio W, Tan K, Sonnenberg A, Wei Y, Vu TH. Integrin α6β4 identifies an adult distal lung epithelial population with regenerative potential in mice. J Clin Invest. 2011;121(7):2855-62.

21. Sinha M, Lowell CA. Isolation of highly pure primary mouse alveolar epithelial type II cells by flow cytometric cell sorting. Bio-protocol. 2016;6(22):e2013.

22. Vaughan AE, Brumwell AN, Xi Y, Gotts JE, Brownfield DG, Treutlein B, Tan K, Tan V, Liu FC, Looney MR. Lineage-negative progenitors mobilize to regenerate lung epithelium after major injury. Nature. 2015;517(7536):621-5.

23. Weiner AI, Zhao G, Zayas HM, Holcomb NP, Adams-Tzivelekidis S, Wong J, Gentile ME, Reddy D, Wei J, Palashikar G. ΔNp63 drives dysplastic alveolar remodeling and restricts epithelial plasticity upon severe lung injury. Cell reports. 2022;41(11):111805.

24. Zacharias WJ, Frank DB, Zepp JA, Morley MP, Alkhaleel FA, Kong J, Zhou S, Cantu E, Morrisey EE. Regeneration of the lung alveolus by an evolutionarily conserved epithelial progenitor. Nature. 2018;555(7695):251-5.

25. Liberti DC, Kremp MM, Liberti III WA, Penkala IJ, Li S, Zhou S, Morrisey EE. Alveolar epithelial cell fate is maintained in a spatially restricted manner to promote lung regeneration after acute injury. Cell reports. 2021;35(6):109092.

26. Nureki S, Tomer Y, Venosa A, Katzen J, Russo SJ, Jamil S, Barrett M, Nguyen V, Kopp M, Mulugeta S. Expression of mutant Sftpc in murine alveolar epithelia drives spontaneous lung fibrosis. J Clin Invest. 2018;128(9):4008-24.

27. Di Tommaso P, Chatzou M, Floden EW, Barja PP, Palumbo E, Notredame C. Nextflow enables reproducible computational workflows. Nat Biotechnol. 2017;35(4):316-9.

28. Ewels PA, Peltzer A, Fillinger S, Patel H, Alneberg J, Wilm A, Garcia MU, Di Tommaso P, Nahnsen S. The nf-core framework for community-curated bioinformatics pipelines. Nat Biotechnol. 2020;38(3):276-8.

29. Love MI, Huber W, Anders S. Moderated estimation of fold change and dispersion for RNA-seq data with DESeq2. Genome Biol. 2014;15(12):1-21.

30. Wolf FA, Angerer P, Theis FJ. SCANPY: Large-scale single-cell gene expression data analysis. Genome Biol. 2018;19:1-5.

31. Noureen N, Ye Z, Chen Y, Wang X, Zheng S. Signature-scoring methods developed for bulk samples are not adequate for cancer single-cell RNA sequencing data. Elife. 2022;11:e71994.

32. Miller I, Min M, Yang C, Tian C, Gookin S, Carter D, Spencer SL. Ki67 is a graded rather than a binary marker of proliferation versus quiescence. Cell reports. 2018;24(5):1105,1112. e5.

33. Barkauskas CE, Cronce MJ, Rackley CR, Bowie EJ, Keene DR, Stripp BR, Randell SH, Noble PW, Hogan BL. Type 2 alveolar cells are stem cells in adult lung. J Clin Invest. 2013;123(7):3025-36.

34. Flaherty KR, Travis WD, Colby TV, Toews GB, Kazerooni EA, Gross BH, Jain A, STRAWDERMAN III RL, Flint A, LYNCH III JP. Histopathologic variability in usual and nonspecific interstitial pneumonias. American journal of respiratory and critical care medicine. 2001;164(9):1722-7.

35. Thannickal VJ, Horowitz JC. Evolving concepts of apoptosis in idiopathic pulmonary fibrosis. Proceedings of the American Thoracic Society. 2006;3(4):350-6.

36. Zhang D, Povysil G, Kobeissy PH, Li Q, Wang B, Amelotte M, Jaouadi H, Newton CA, Maher TM, Molyneaux PL. Rare and common variants in KIF15 contribute to genetic risk of idiopathic pulmonary fibrosis. American journal of respiratory and critical care medicine. 2022;206(1):56-69.

37. Alder JK, Barkauskas CE, Limjunyawong N, Stanley SE, Kembou F, Tuder RM, Hogan BL, Mitzner W, Armanios M. Telomere dysfunction causes alveolar stem cell failure. Proceedings of the National Academy of Sciences. 2015;112(16):5099-104.

38. Lehmann M, Korfei M, Mutze K, Klee S, Skronska-Wasek W, Alsafadi HN, Ota C, Costa R, Schiller HB, Lindner M. Senolytic drugs target alveolar epithelial cell function and attenuate experimental lung fibrosis ex vivo. European Respiratory Journal. 2017;50(2)

39. Yao C, Guan X, Carraro G, Parimon T, Liu X, Huang G, Mulay A, Soukiasian HJ, David G, Weigt SS. Senescence of alveolar type 2 cells drives progressive pulmonary fibrosis. American Journal of Respiratory and Critical Care Medicine. 2021;203(6):707-17.

40. Schafer MJ, White TA, Iijima K, Haak AJ, Ligresti G, Atkinson EJ, Oberg AL, Birch J, Salmonowicz H, Zhu YI. Cellular senescence mediates fibrotic pulmonary disease. Nature communications. 2017;8(1):1-11.

41. Atochina-Vasserman EN, Bates SR, Zhang P, Abramova H, Zhang Z, Gonzales L, Tao J, Gochuico BR, Gahl W, Guo C. Early alveolar epithelial dysfunction promotes lung inflammation in a mouse model of Hermansky-Pudlak syndrome. American journal of respiratory and critical care medicine. 2011;184(4):449-58.

42. Young LR, Gulleman PM, Short CW, Tanjore H, Sherrill T, Qi A, McBride AP, Zaynagetdinov R, Benjamin JT, Lawson WE. Epithelial-macrophage interactions determine pulmonary fibrosis susceptibility in Hermansky-Pudlak syndrome. JCI insight. 2016;1(17)

43. Rouhani FN, Brantly ML, Markello TC, Helip-Wooley A, O'Brien K, Hess R, Huizing M, Gahl WA, Gochuico BR. Alveolar macrophage dysregulation in Hermansky-Pudlak syndrome type 1. American journal of respiratory and critical care medicine. 2009;180(11):1114-21.

44. Gochuico BR, Dorward H, Franklin T, O'Brien K, Gahl W, Malicdan M, Han C. Shortened Telomeres in Type II Alveolar Epithelial Cells in Hermansky-Pudlak Syndrome Pulmonary Fibrosis In: C59. Genetic and Epigenetic Mechanisms in Pulmonary Fibrosis. American Thoracic Society; 2019 p. A5267.

45. Nakatani Y, Nakamura N, Sano J, Inayama Y, Kawano N, Yamanaka S, Miyagi Y, Nagashima Y, Ohbayashi C, Mizushima M. Interstitial pneumonia in Hermansky-Pudlak syndrome: Significance of florid foamy swelling/degeneration (giant lamellar body degeneration) of type-2 pneumocytes. Virchows Archiv. 2000;437(3):304-13.

46. Kook S, Wang P, Meng S, Jetter CS, Sucre JM, Benjamin JT, Gokey JJ, Hanby HA, Jaume A, Goetzl L. AP-3–dependent targeting of flippase ATP8A1 to lamellar bodies suppresses activation of YAP in alveolar epithelial type 2 cells. Proceedings of the National Academy of Sciences. 2021;118(20)

47. Weng T, Poth JM, Karmouty-Quintana H, Garcia-Morales LJ, Melicoff E, Luo F, Chen N, Evans CM, Bunge RR, Bruckner BA. Hypoxia-induced deoxycytidine kinase contributes to epithelial proliferation in pulmonary fibrosis. American journal of respiratory and critical care medicine. 2014;190(12):1402-12.

48. Summer R, Krishna R, Schriner D, Cuevas-Mora K, Sales D, Para R, Roman J, Nieweld C, Gochuico BR, Romero F. Matrix metalloproteinase activity in the lung is increased in Hermansky-Pudlak syndrome. Orphanet journal of rare diseases. 2019;14(1):1-11.

49. Kobayashi Y, Tata A, Konkimalla A, Katsura H, Lee RF, Ou J, Banovich NE, Kropski JA, Tata PR. Persistence of a regeneration-associated, transitional alveolar epithelial cell state in pulmonary fibrosis. Nat Cell Biol. 2020;22(8):934-46.

50. Strunz M, Simon LM, Ansari M, Kathiriya JJ, Angelidis I, Mayr CH, Tsidiridis G, Lange M, Mattner LF, Yee M. Alveolar regeneration through a Krt8 transitional stem cell state that persists in human lung fibrosis. Nature communications. 2020;11(1):1-20.

**Figure Legends**

**Figure 1: Loss of alveolar type II epithelial (AT2) cells with aging in HPS mice.** (A) Representative immunofluorescence (IF) staining of whole-mount lung issue for proSP-C in WT and HPS1/2 mice at 60 weeks of age. (B) Representative IF staining of paraffin-embedded lung tissue for proSP-C in WT, HPS1/2, HPS1, and HPS2 mice at 8 and 48 weeks of age. (C-E) Quantification of percentage of proSP-$C^+$ cells as a percentage of total cells (by DAPI) in WT vs. (C) HPS1/2, (D) HPS1, and (E) HPS2 mice at 4, 8, 24, and 48 weeks of age. DAPI stains nuclei (blue). All quantification data are represented as mean ± SEM. Two-tailed t tests: ns, not significant; adjusted * $p < .05$; ** $p < .01$; *** $p < .001$; n = 4-6 per group per time point. Scale bars for whole mount IF images, 50 µm; for paraffin-embedded IF images, 20 µm.

**Figure 2: Lineage tracing of alveolar type II epithelial (AT2) cells in HPS1 and HPS2 confirms loss of AT2 cells with aging.** (A) Representative immunofluorescence staining of paraffin-embedded lung tissue for proSP-C and the lineage trace marker EYFP in WT Sftpc$^{CreERT2/+}$;R26R$^{EYFP/+}$, HPS1 Sftpc$^{CreERT2/+}$;R26R$^{EYFP/+}$, and HPS2 Sftpc$^{CreERT2/+}$;R26R$^{EYFP/+}$ mice at 8 and 24 weeks of age. (B, C) Quantification of percentage of proSP-$C^+$ lineage-traced cells as a percentage of total cells in WT Sftpc$^{CreERT2/+}$;R26R$^{EYFP/+}$ vs. (B) HPS1 Sftpc$^{CreERT2/+}$;R26R$^{EYFP/+}$ and (C) HPS2 Sftpc$^{CreERT2/+}$;R26R$^{EYFP/+}$ mice at 8 and 24 weeks of age. DAPI stains nuclei (blue). All quantification data are represented as mean ± SEM. Two-tailed t tests: ns, not significant; adjusted * $p < .05$; ** $p < .01$; n = 4-6 per group per time point. All scale bars, 20 µm.

**Figure 3: HPS2 lung organoids demonstrate attenuated size and growth.** (A) Representative brightfield images of lung organoids generated with alveolar type II epithelial (AT2) cells isolated from WT, HPS1, and HPS2 mice with WT fibroblasts at day 9 (D9) and day 21 (D21) of culture. (B) Representative immunofluorescence imaging of whole-mount organoids with WT, HPS1, and HPS2 AT2 cells for proSP-C and AGER at D21 of culture. (C) Quantification of WT, HPS1, and HPS2 organoid size from D9 to D21 of culture. Each point represents the average of lung organoids derived from n = 3 mice per group. (D) Quantification of WT, HPS1, and HPS2 organoid colony forming efficiency (CFE) at D21 of culture. Each point represents the average of at least three replicate wells from one mouse for a total of n = 3 mice per group. DAPI stains nuclei (blue). All quantification data are represented as mean ± SEM. Two-tailed t tests: ns, not significant; * $p < .05$. All scale bars, 20 µm.

**Figure 4: HPS1 alveolar type II epithelial (AT2) cell proliferation is impaired after acute influenza infection.** (A) Mean change in weight and (B) oxygen saturation in WT and HPS1 mice from 0 to 14 dpi. (C) Representative images demonstrating computational image analysis approach to define regions of lung injury from H&E-stained lung sections. (D) Representative immunofluorescence staining of paraffin-embedded lung tissue for proSP-C and EdU in WT and HPS1 mice at 14 dpi in severely and mildly injured regions. (E) Quantification of the percentage of EdU-positive AT2 cells (by proSP-C staining) in WT and HPS1 mice at 14 dpi in mildly injured and severely injured regions. All quantification data are represented as mean ± SEM. Two-tailed t tests: * $p < .05$; n = 6-8 per group per time point. All scale bars, 20 µm.

**Figure 5: HPS2 alveolar type II epithelial (AT2) cell proliferation is impaired after acute influenza infection.** (A) Mean change in weight and (B) oxygen saturation in WT and HPS2 mice from 0 to 14 dpi. (C) Representative images demonstrating computational image analysis approach to define regions of lung injury from H&E-stained lung sections. (D) Representative immunofluorescence staining of paraffin-embedded lung tissue for proSP-C and EdU in WT and HPS2 mice at 14 dpi in severely and mildly injured regions. (E) Quantification of the percentage of EdU-positive AT2 cells (by proSP-C staining) in WT and HPS2 mice at 14 dpi in mildly injured and severely injured regions. All quantification data are represented as mean ± SEM. Two-tailed t tests: ns, not significant; * $p < .05$; n = 3-4 per group per time point. All scale bars, 20 µm.

**Figure 6: Transcriptomic analysis suggests subpopulations of proliferating and senescent HPS alveolar type II epithelial (AT2) cells.** (A) Matrixplot of top genes over- and under-expressed in AT2 cells from WT and HPS1/2 mice at 8 and 48 weeks of age and HPS1 and HPS2 mice at 8 weeks of age. (B) Differential expression analysis of selected proliferation and senescence-associated genes. (C) Overall gene set score for cellular senescence. (D) β-galactosidase staining of AT2 cells isolated from WT and HPS1/2 mice at 48 weeks of age. n = 4 per group per time point. All scale bars, 50 µm.

**Supplemental Figure Legends**

**Supplemental Figure 1: Progressive fibrosis with aging in HPS1/2 mice.** (A-C) Representative (A) H&E, (B) trichrome, and (C) picrosirius red stained images from WT and HPS1/2 mice at 8 and 48 weeks of age. (D) Quantification of the percentage of collagen detected by picrosirius red staining in WT and HPS1/2 mice at 8, 24, and 48 weeks of age. All quantification data are represented as mean ± SEM. Two-tailed t tests: ns, not significant; * $p < .05$; n = 4-6 per group per time point. All scale bars, 20 µm.

**Supplemental Figure 2: Quantification of alveolar type II epithelial (AT2) cells as a percentage of total epithelial cells in HPS1 and HPS2 mice.** (A-B) Representative immunofluorescence staining of paraffin-embedded lung tissue for proSP-C and Nkx2.1 in (A) WT and HPS1 mice at 8 weeks of age and (B) WT and HPS2 mice at 24 weeks of age. (C-D) Quantification of percentage of proSP-C$^+$ Nkx2.1$^+$ cells as a percentage of total epithelial cells (by Nkx2.1$^+$ cells) in (C) WT vs. HPS1 mice at 8 weeks of age and (D) WT vs. HPS2 mice at 24 weeks of age. DAPI stains nuclei (blue). All quantification data are represented as mean ± SEM. Two-tailed t tests: ns, not significant; * $p < .05$, ** $p < .01$; n = 4 per group per time point. All scale bars, 20 µm.

**Supplemental Figure 3: Quantification of alveolar type II epithelial (AT2) cells with aging in HPS3 and epithelial transgenic-corrected (TG) HPS2 mice.** (A) Representative immunofluorescence staining of paraffin-embedded lung tissue for proSP-C in WT, HPS3, and transgenic (TG) HPS2 mice at 8 and 24 weeks of age. (B) Quantification of percentage of proSP-C$^+$ cells as a percentage of total cells (by DAPI staining) in WT vs. HPS3 mice at 8 and 24 weeks of age. (C) Quantification of percentage of proSP-C$^+$ cells as a percentage of total cells (by DAPI staining) in WT vs. TG HPS2 mice at 24 weeks of age. DAPI stains nuclei (blue). All quantification data are represented as mean ± SEM. Two-tailed t tests: ns, not significant; * $p < .05$; n = 4 per group per time point. All scale bars, 20 µm.

**Supplemental Figure 4: Krt5$^+$ cells in acute influenza infection.** (A) Representative immunofluorescence staining of lung tissue for keratin 5 (Krt5) in WT, HPS1, and HPS2 mice at 14 days post infection (dpi) with influenza. (B-C) Quantification of Krt5$^+$ area as a percentage of total lung area in (B) WT vs. HPS1 mice and (C) WT vs. HPS2 mice at 14 dpi. DAPI stains nuclei (blue). Two-tailed t tests: ns, not significant; n = 3-7 per group per time point. Scale bar of tile scans, 2 cm; inset, 20 µm.

**Supplemental Figure 5: Reduced AT2 cell percentage in HPS mice with aging by fluorescence activated cell sorting (FACS).** (A-B) Representative FACS plots of AT2 cell population in (A) WT and (B) HPS1/2 mice at 8 weeks of age. (C) Quantification of percentage of CD45$^-$ EpCAM$^+$ CD104$^-$ live cells in WT and HPS1/2 mice at 8 and 48 weeks of age. (D) proSP-C immunostaining of cytospin preparations from AT2 cells isolated from WT and HPS1/2 mice at 8 weeks of age. DAPI stains nuclei (blue). Two-tailed t tests: *** $p < .001$; **** $p < .0001$; n = 4-5 per group per time point. All scale bars, 50 µm.

**Supplemental Figure 6: Differential gene expression analysis of WT vs. HPS AT2 cells.** (A-C) Volcano plots showing the log2-fold changes (LFCs) in gene expression as a function of genotype in (A) HPS1, (B) HPS2, and (C) HPS1/2 vs. WT AT2 cells. (D-I) Over-representation analysis (ORA) from gProfiler showing GO: Biological Processes (GO:BP) associated with genes upregulated in (D) HPS1, (F) HPS2, and (H) HPS1/2 vs. WT AT2 cells and downregulated in (E) HPS1, (G) HPS2, and (I) HPS1/2 vs. WT AT2 cells.

**Figure 1**

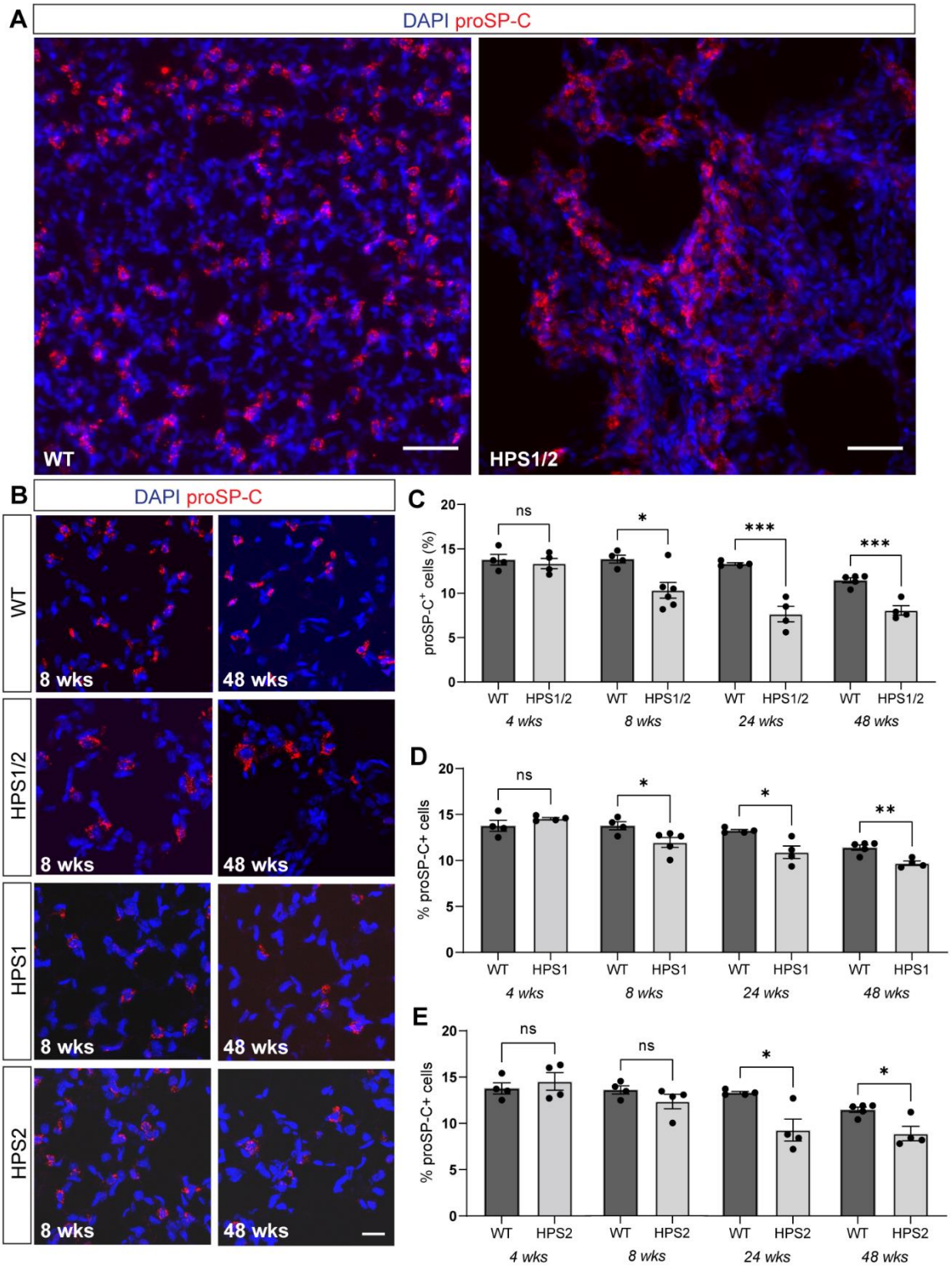
A
DAPI proSP-C
WT
HPS1/2
B
DAPI proSP-C
WT
HPS1/2
HPS1
HPS2
8 wks
48 wks
C
proSP-C+ cells (%)
ns
*
***
***
WT
HPS1/2
4 wks
8 wks
24 wks
48 wks
D
% proSP-C+ cells
ns
*
*
**
WT
HPS1
4 wks
8 wks
24 wks
48 wks
E
% proSP-C+ cells
ns
ns
*
*
WT
HPS2
4 wks
8 wks
24 wks
48 wks

**Figure 2**

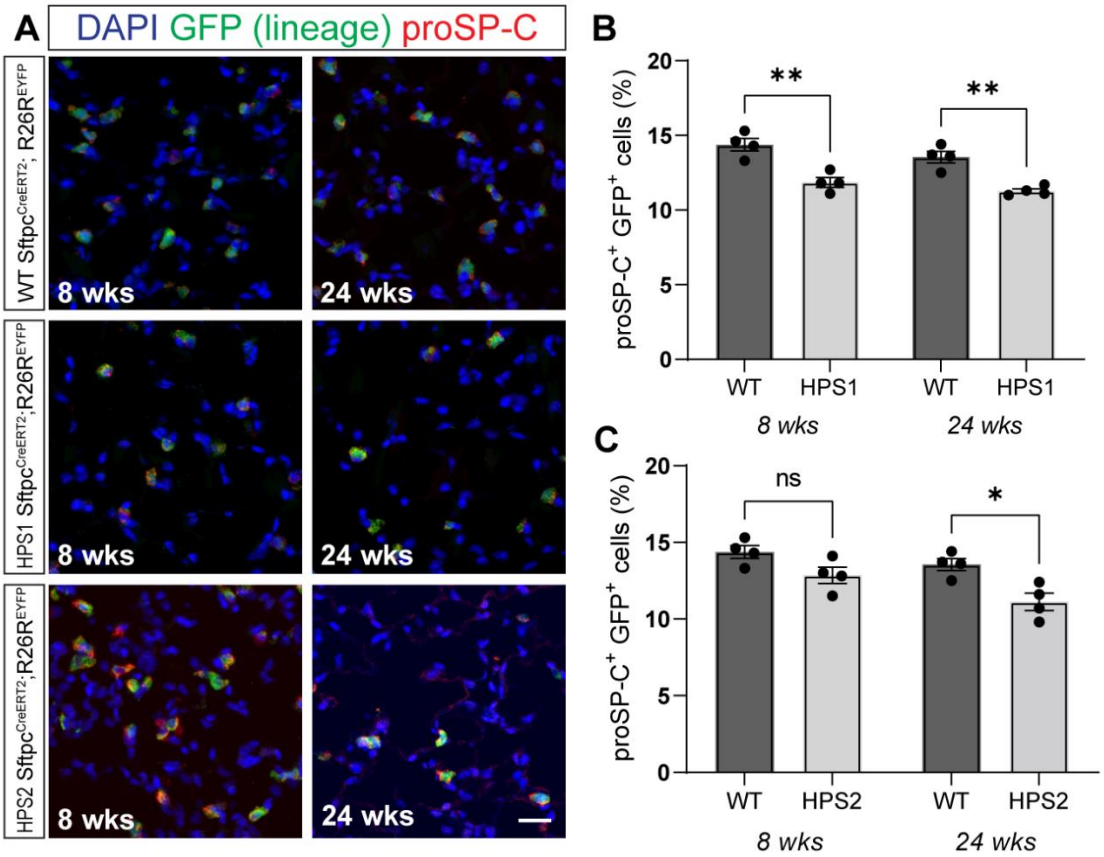
A
DAPI GFP (lineage) proSP-C
WT SftpcCreERT2; R26REYFP
HPS1 SftpcCreERT2;R26REYFP
HPS2 SftpcCreERT2;R26REYFP
8 wks
24 wks
B
proSP-C+ GFP+ cells (%)
**
**
WT
HPS1
8 wks
24 wks
C
ns
*
WT
HPS2
8 wks
24 wks

**Figure 3**

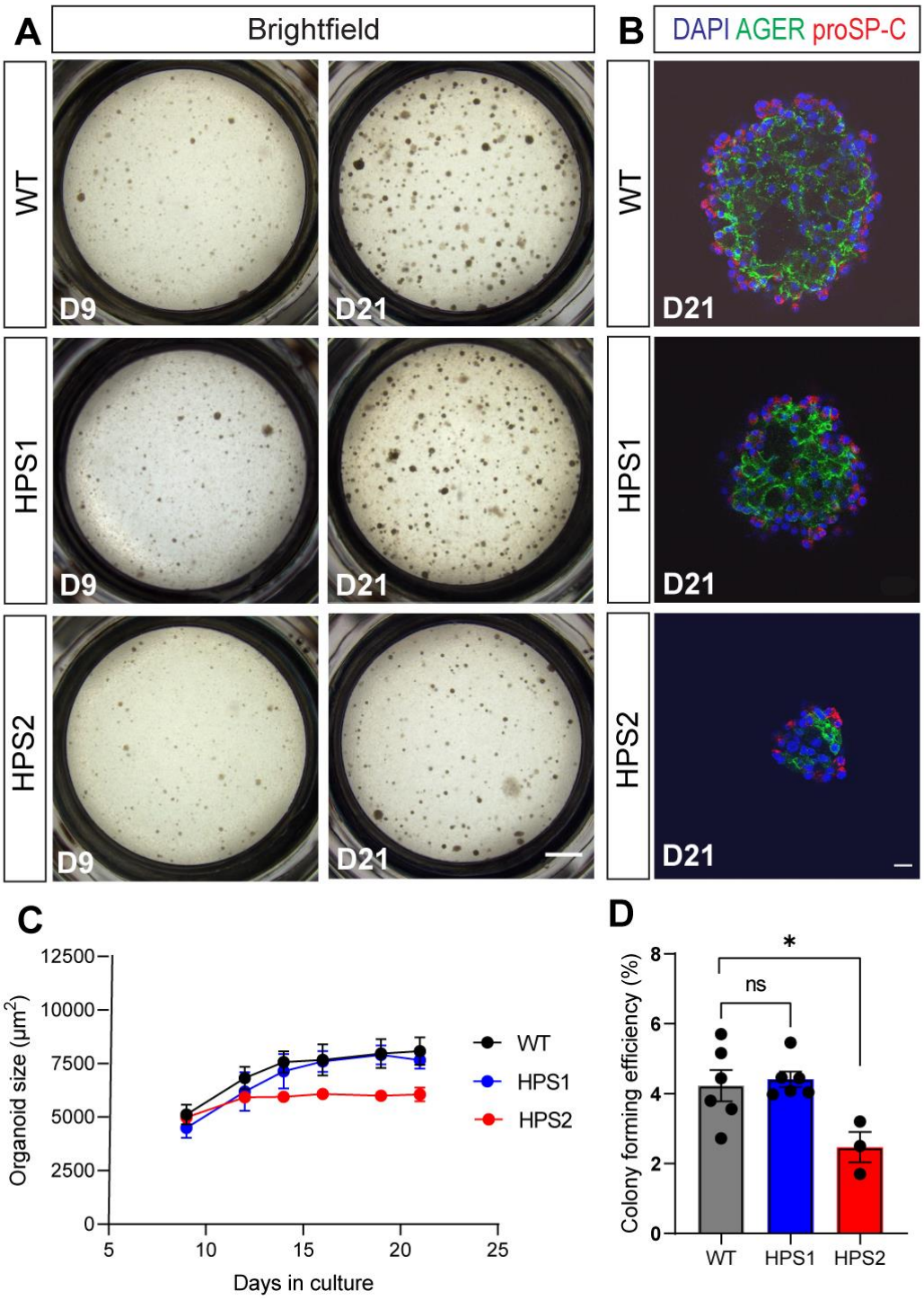
A
Brightfield
WT
HPS1
HPS2
D9
D21
B
DAPI AGER proSP-C
C
Organoid size (μm²)
Days in culture
WT
HPS1
HPS2
D
Colony forming efficiency (%)
ns
*

**Figure 4**

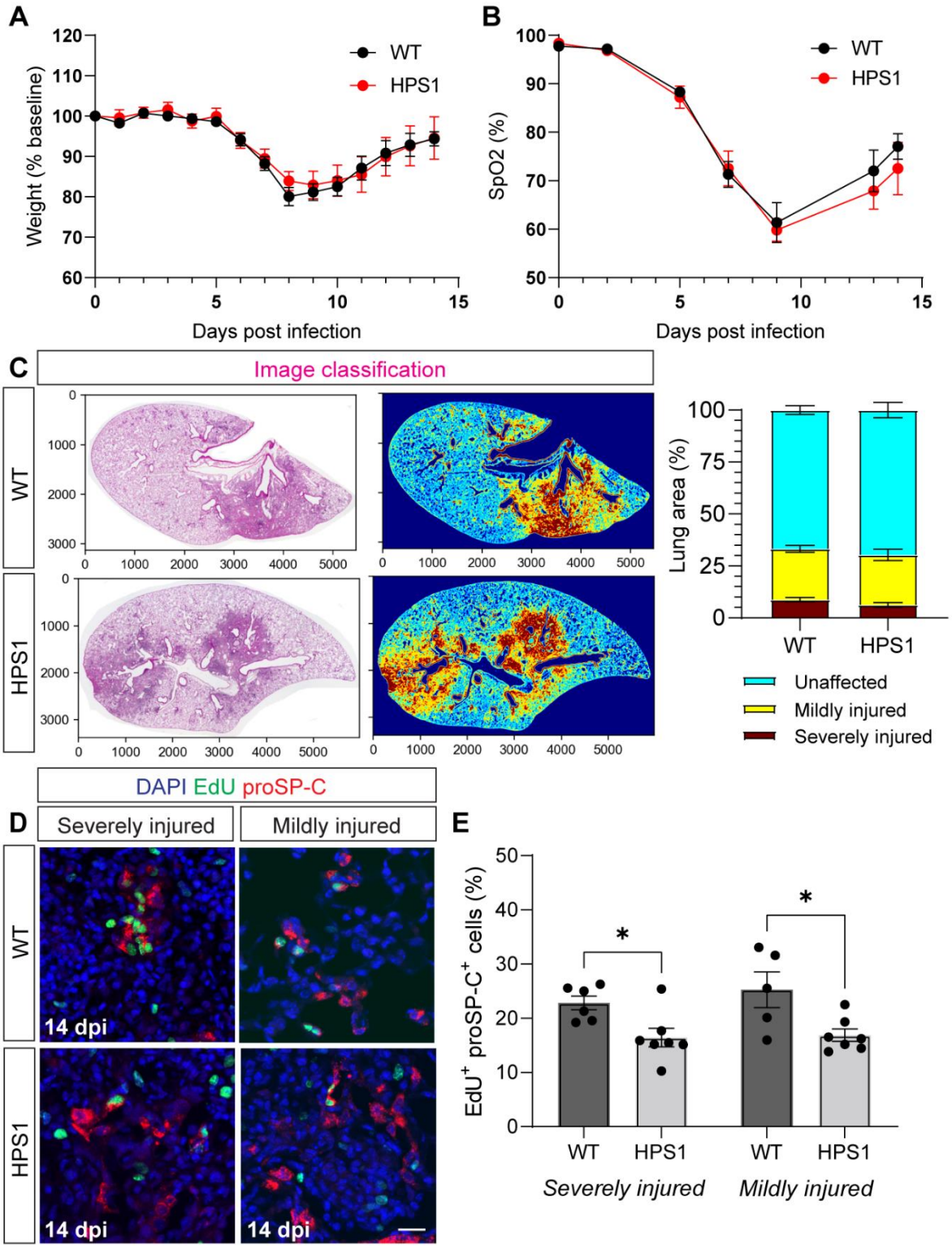
A
Weight (% baseline)
Days post infection
WT
HPS1
B
SpO2 (%)
Days post infection
WT
HPS1
C
Image classification
WT
HPS1
Lung area (%)
WT
HPS1
Unaffected
Mildly injured
Severely injured
DAPI EdU proSP-C
D
Severely injured
Mildly injured
WT
HPS1
14 dpi
E
EdU+ proSP-C+ cells (%)
WT
HPS1
Severely injured
Mildly injured

**Figure 5**

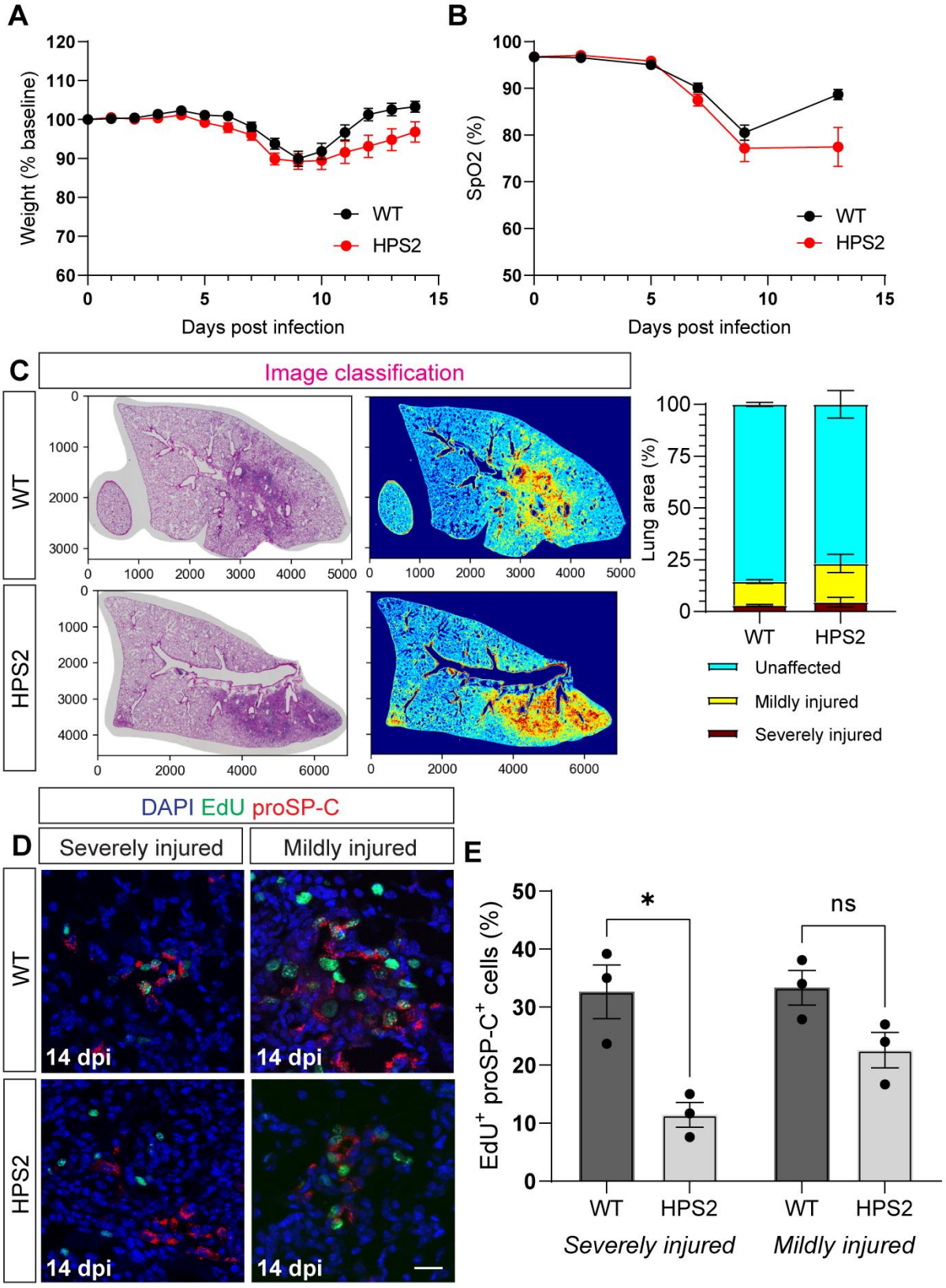
A
Weight (% baseline)
Days post infection
WT
HPS2
B
SpO2 (%)
Days post infection
WT
HPS2
C
Image classification
WT
HPS2
Lung area (%)
WT
HPS2
Unaffected
Mildly injured
Severely injured
DAPI EdU proSP-C
D
Severely injured
Mildly injured
WT
HPS2
14 dpi
E
EdU+ proSP-C+ cells (%)
*
ns
WT
HPS2
Severely injured
Mildly injured

**Figure 6**

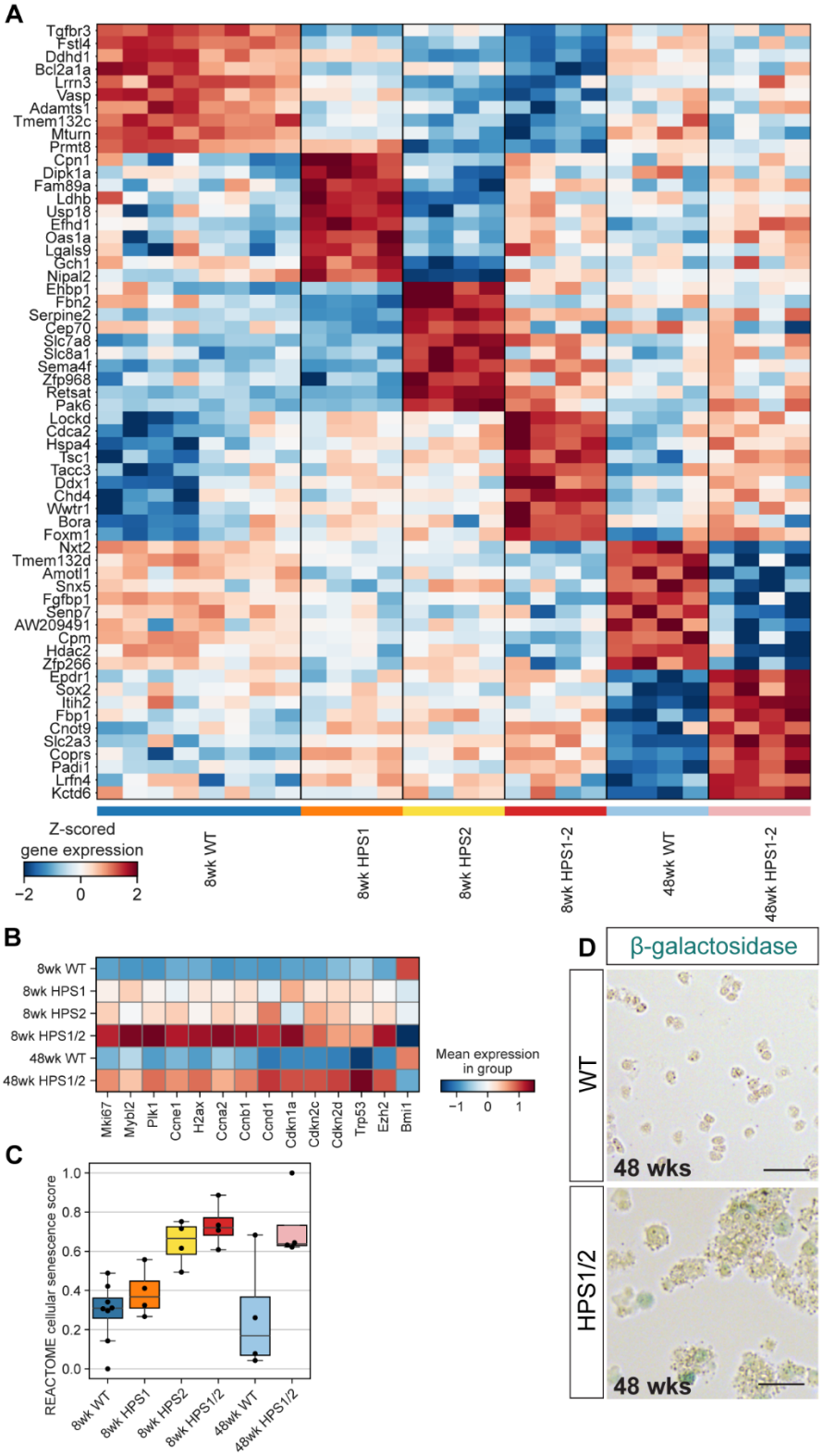
A
Tgfbr3
Fstl4
Ddhd1
Bcl2a1a
Lrrn3
Vasp
Adamts1
Tmem132c
Mturn
Prmt8
Cpn1
Dipk1a
Fam89a
Ldhb
Usp18
Efhd1
Oas1a
Lgals9
Gch1
Nipal2
Ehbp1
Fbn2
Serpine2
Cep70
Slc7a8
Slc8a1
Sema4f
Zfp968
Retsat
Pak6
Lockd
Cdca2
Hspa4
Tsc1
Tacc3
Ddx1
Chd4
Wwtr1
Bora
Foxm1
Nxt2
Tmem132d
Amotl1
Snx5
Fgfbp1
Senp7
AW209491
Cpm
Hdac2
Zfp266
Epdr1
Sox2
Itih2
Fbp1
Cnot9
Slc2a3
Coprs
Padi1
Lrfn4
Kctd6
Z-scored
gene expression
−2
0
2
8wk WT
8wk HPS1
8wk HPS2
8wk HPS1-2
48wk WT
48wk HPS1-2
B
8wk WT
8wk HPS1
8wk HPS2
8wk HPS1/2
48wk WT
48wk HPS1/2
Mki67
Mybl2
Plk1
Ccne1
H2ax
Ccna2
Ccnb1
Ccnd1
Cdkn1a
Cdkn2c
Cdkn2d
Trp53
Ezh2
Bmi1
Mean expression
in group
−1
0
1
C
REACTOME cellular senescence score
1.0
0.8
0.6
0.4
0.2
0.0
8wk WT
8wk HPS1
8wk HPS2
8wk HPS1/2
48wk WT
48wk HPS1/2
D
β-galactosidase
WT
48 wks
HPS1/2
48 wks